Preparation and Characterization of Nicke-iron Alloy Film as Freestanding Electrode for Oxygen Evolution Reaction

Mengqi Yao[1], Weilin Chen[2] and Wencheng Hu[1]

[1] *State Key Laboratory of Electronic Thin Films and Integrated Devices, University of Electronic Science & Technology of China, Chengdu 610054, China*

[2] *CNPC Beijing Richfit Information Technology Co. Ltd., Beijing 100007, China*

Abstract. This work reports the porous nicke-iron alloy film supported on stainless steel mesh as freestanding electrode for enhanced oxygen evolution reaction (OER) catalyst prepared from an one step electrodeposition method. Results indicated that the porous nickle-iron alloy film exhibits a low overpotential of 270 mV at 10 mA cm^{-2} and excellent electroconductibility. The superior OER properties can be attributed to its novel synthetic process, conductive substrate and porous structure. This work will provide a new strategy to fabricate alloy film for OER electrocatalyst.

1 Introduction

Hydrogen has been considered as a promising alternative to fossil fuels [1-3]. As our known, electrochemical water spliting is an efficient way to generate hydrogen [4,5]. Oxygen evolution reaction (OER) electrolysis, as an important reaction involved in water splitting, has attracted increasing attention for clean energy generation and efficient energy storage. The oxygen evolution reaction significantly influence the efficiency of overall water splitting due to its rough four electrons kinetic process [6,7]. Noble metal catalysts including RuO_2 and IrO_2 have been identified as efficient OER catalysts because of their low overpotential and small Tafel slope. However, the high cost, poor cycling stability and toxicity limit their large scale applications. First-row transition metal based materials have attracted enormous attentions for OER catalysts due to their low cost and high catalytic activity based on earth-abundant metals [8,9]. Among first-row transition metal materials, nickle and iron based materials possesses outstanding properties including relatively high electrical conductivity and highly catalytic performances for oxygen evolution reacion, making it potential candidates for OER catalysts [10-13]. However, NiFe based electrocatalysts mentioned in recent literatures, own low stability and poor conductivity [14-19]. Therefore, fabricating NiFe materials with enhanced OER properties attracts plenty of interests.

Recently, there were many discoveries and recent progresses being explored to improve OER catalytic activities. Scientists fabricated different microstructure and micromorophology by different methods to increase specific surface area and active sites to improve OER properties. Moreover, different elements were doped into NiFe based materials to increase defects in order to improve electrical conductivity of system. Meanwhile, combining conductive materials, such as graphene and Ag particles, with electroactive materias not only boost conductivity, but it also can expose more edge defects. For instance, Lu and his coworkers demonstrated that a three-dimensional (3D) architecture of NiFe layered double hydroxide (NiFe-LDH) significantly reduced the onset potential, yielded high current density at small overpotentials, and showed outstanding cycling stability in electrochemical oxygen evolution reaction [20]. Feng and his coworkers fabricated a of freestanding sandwiched NiFe nanoparticles encapsulated by graphene sheets with a low onste potential of 1.44 V (vs. RHE) [21]. Qi and his coworkers prepared highly porous nickle and iron oxide with improved crystallinity. The catalysts showed small overpotential, low Tafel slope and good stability for OER [22].

Most NiFe based OER catalysts are powders, which reported in the recent studies [23-26]. The binders, such as Nafion solution, were utilized to promote electroactive materials powders coating onto the surface of conductive substrates including Ni foam, carbon cloth and stainless steel mesh. However, the uses of binders significantly reduce the conductivity of the system. In other words, using binder will impede the transfer of ions and mass, giving rise to degraded OER performance. It is a common phenomenon that the glued OER powders always peel off easily during long-time electrochemical tests, since the influence of gas evolution on the surface of electrode [27]. Metal alloys, growing onto the surface of conductive

substrates by electrodeposition method, have been wildly employed as high performance electrocatalysts. Although above mentioned metal alloy films own relatively high OER propertied compared with glued OER powder, the coatings usually show general electrocatalytic performance and stability, for the reason that the alloy film possesses little active sites and only the surface layers of electroactive materials are in contact with electrolyte. Therefore, exploring a new strategy to electrodeposit metal alloy filmwith abundant active sites for OER catalysts is of great interest.

In this study, porous nicke-iron alloy film supported on stainless steel mesh was synthesized by an one step electrodeposition method. We studied the OER properties of porous nickle-iron alloy films. We concluded that the one step electrodeposition method has advantages for oxygen evolution reaction as follows: (1) abundant active sites and large specific surface area; (2) relatively excellent crystallinity and improved cycling stability. The nicke-iron alloy film exhibits a low overpotential of 270 mV at a current density of 10 mA cm^{-2} and significantly improved electroconductibility, suggesting an enhanced OER property. The superior OER properties can be attributed to its novel synthetic process, conductive substrate and porous structure. This work will provide a new strategy to fabricate alloy film for OER electrocatalyst.

2 Experimental sections

2.1 Materials

Nickel sulfate hexahydrate ($NiSO_4 \cdot 6H_2O$), iron sulfate hexahydrate ($FeSO_4 \cdot 6H_2O$), boric acid (H_3BO_3), potassium hydroxide (KOH), ethyl alcohol (C_2H_5OH) and methanol solution (HCHO) were obtained from Chengdu Kelong Chemical Reagent Co. (Chengdu, China). Stainless steel mesh (304L, 300 mesh) and Ni foil were purchased from Chengdu Jinshan Chemical Reagent Co. (Chengdu, China). Ni foil (thickness: 1 mm) and deionized water with resistivity of 18.2 MΩ cm were used as counter electrode and solvent, respectively.

2.2 Preparation of nicke-iron alloy film

All chemicals were used as received without any further purification. The binary nickle-iron alloy film was prepared via a novel electrodeposition method. Briefly, 6.3g nickel sulfate hexahydrate ($NiSO_4 \cdot 6H_2O$), 3.3g iron sulfate hexahydrate ($FeSO_4 \cdot 6H_2O$) and 1.2 g boric acid (H_3BO_3) were dissolved in 65 ml distilled water. In addition, 5 ml methanol (HCHO) as reductant was added into the solution. The solution was stirred for 30min under magnetic condition. Then the transparent solution was transferred into a 100ml electroplating bath. A 2 cm×2 cm of stainless steel mesh (304L, 300 mesh) was used as cathode; 2 cm×2 cm nickel foil was used as anode. Prior to the electrodeposition process, the stainless steel mesh substrate was cleaned in 1 M HCl solution under ultrasonication condition for 10 min to remove oxide layer on the surface, and washed sequentially by deionized water and ethyl alcohol for several times. The electrodeposition systrm was put inside the oven at 60 °C for 10 minutes at the current density of 30 mA cm^{-2}. Then, the as-prepared nickle-iron alloy film was washed with distilled water, ethanol and acetone for six times and dried at 100 °C under vacuum condition. The obtained nickle-iron alloy film supported on stainless steel mesh was used for further materials characterizations and electrochemical tests.

3 Characterizations

The crystalline phase was characterized by X-ray diffractometer (Smartlab9, Pigaku, Japan.). The FESEM were used to evaluated micromorphologies and microstructure operated at 3.0 kV (Inspect F, FEI Co., U.S.).

The OER properties of electrode were characterized by the electrochemical station (PGSTAT302N, Netherlands) under a standard three-electrode system. 1.0 M KOH solution saturated by O_2 was used as electrolyte, 1cm×1cm nicke-iron alloy film supported on stainless steel mesh was used as a freestanding working electrode. Pt/C wire and Hg/HgO electrode was used as counter electrode and reference electrode, respectively. Linear sweep voltammetry (LSV) was performed in 1.0 M KOH solutions from 0 to 1.0 V at a scan rate of 2 mV s^{-1}. Electrochemical impedance spectroscopy (EIS) was measured at open circuit voltages from 10^6 to 10^{-2} Hz. All the potentials in this paper were versus the reversible hydrogen electrode (RHE) according the equation E(RHE) = E(Hg/HgO)+0.059 pH+0.098 V= E(Hg/HgO)+0.0591×14+0.098 V=E(Hg/HgO)+0.9254 V. The overpotential (η) corresponds to the equation η = E(RHE)-1.23 V. All the curves were reported with iR compensation.

4 Results and discussions

4.1 XRD analysis of nicke-iron alloy film

The crystalline structure of porous nicke-iron alloy film supported on stainless steel mesh and blank stainless steel mesh evaluated by X-ray diffractometer (XRD) are shown in Figure 1. The result indicates that the diffraction peaks located at 44.2°, 51.6° are well identified and can be successfully assigned to the (111) and (200) lattice planes of $FeNi_3$ (PDF card: 38-0419). Additionally, compared with the peaks of nicke-iron alloy film, the blank stainless steel mesh substrate shows nearly none obvious peaks, suggesting the phase purity of nicke-iron alloy film supported on stainless steel mesh. We can conclude that nickle-iron alloy is successfully fabricated via on step electrodeposition method. Besides, the particle size of nicke-iron alloy film supported on stainless steel mesh is 12.026 nm calculated by XRD curve using Scherrer equation, confirming a relatively excellent crystallinity.

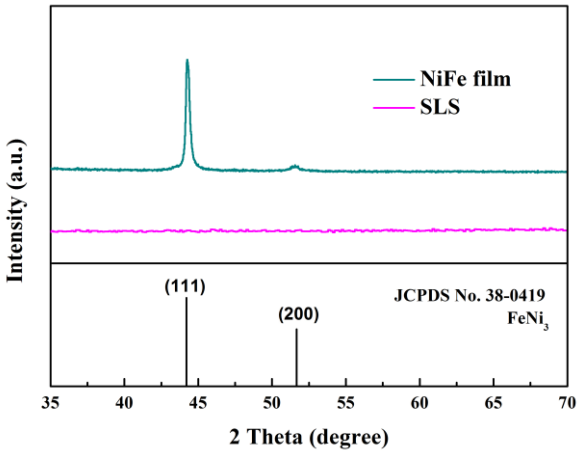

Figure 1. XRD pattern of nicke-iron alloy film and stainless steel mesh.

4.2 Micromorphology characterizations of nicke-iron alloy film

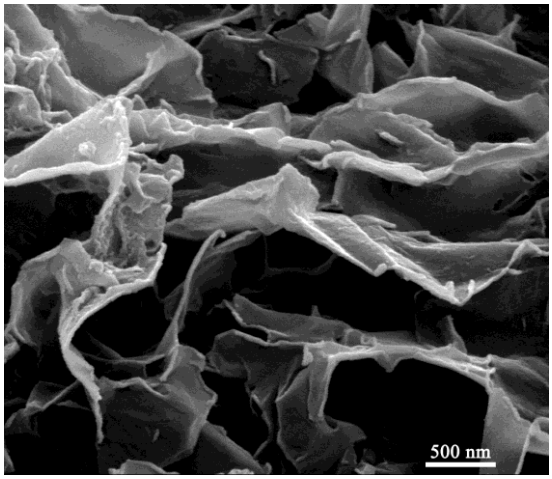

Figure 2. SEM image of nicke-iron alloy film.

Micromorphology and microstructure of porous nicke-iron alloy film supported on stainless steel mesh analyzed by scanning electron microscope (SEM) is shown in Figure 2. It can be observed that the nicke-iron alloy film was successfully electrodeposited on stainless steel mesh. As displayed in Figure 2, the nicke-iron alloy film was composed of relatively homogeneous nanosheets like microstructures. The thickness of each vertical nanosheet is approximately 80-120 nm and the extension of the nanosheets ranged from 200 nm to several thousand nanometers. The nanosheet like micromorphology can provide large specific surface area and abundant electrochemically active sites. The large specific surface area can boost release of O_2 from the surface of nicke-iron alloy film and prevent the film peeling from the surface of substrate under the impact of oxygen release during a long-term stability test, especially under high current density and vigorous gas evolution conditions. In other words, the nanosheet like structure enhance the cycling stability. Meanwhile, large specific surface area can provide more electrochemically active sites for the electrocatalysis leading to significantly enhanced electrocatalytic performance for oxygen evolution reaction [28, 29]. Besides, the nanosheet like micromorphologies also can facilitate diffusion of electron and OH^- and increase the contact area between electrolytes and catalytic active sites, leading to improved electrocatalytic performances.

4.3 OER properties of nicke-iron alloy film

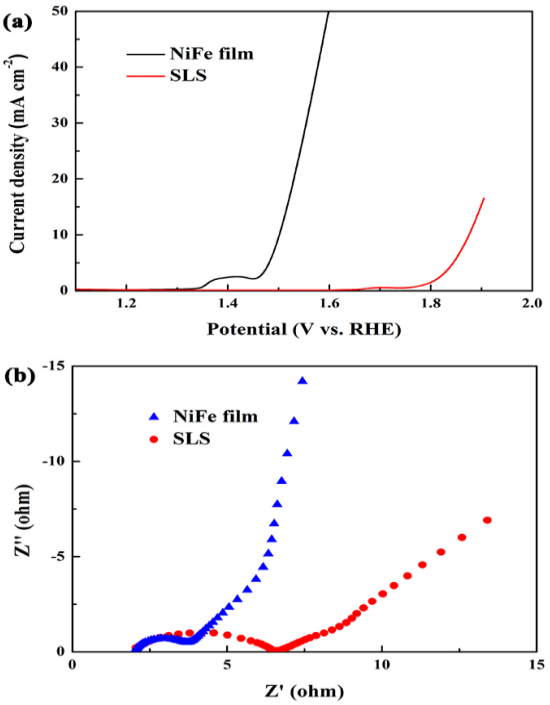

Figure 3. (a) The iR corrected polarization curves of nicke-iron alloy film and stainless steel mesh in 1.0 M KOH. (b) The EIS curves of nicke-iron alloy film and stainless steel mesh.

The electrochemical tests were analyzed under a standard three-electrode system using 1.0 M. Porous nickle-iron alloy film supported on stainless steel mesh was employed as the working electrode, a Hg/HgO was used as the reference electrode and a Pt plate was utilized as the counter electrode. Figure 3a reveals iR-corrected polarization curves of porous nicke-iron alloy film supported on stainless steel mesh and blank stainless steel mesh tested at a scan rate of 5 mV s^{-1}. As our known, the potential obtained at a current density of 10 mA cm^{-2} is a commen way to evaluate the OER property of catalysts. From Figure 3a, it can be demonstrated that nicke-iron alloy film shows a low overpotential of 1.50V (vs. RHE) at a current density of 10 mA cm^{-2}, whereas the stainless steel mesh presents potential of 1.87V (vs. RHE) at 10 mA cm^{-2}. The nicke-iron alloy film possess a low overpotential of 270 mV which is much lower than that of stainless steel mesh. The small oxidation process from LSV curve detected at 1.40 V before the onset of OER is corresponding to the formation of Ni and Fe species, which are the active sites to catalyse OER. The results

indicate that the nicke-iron alloy film possesses higher electrocatalytic activity compared with stainless steel mesh due to its large specific surface area, abundant electrochemical active sites and synergistic effect of Ni and Fe atoms. The OER performance is superior to the recent studies. For example, Liu et al. fabricated mesoporous $NiFe_2O_4$ nanorods as efficient oxygen evolution catalyst, which shows overpotential of 342 mV at a current density of 10 mA cm^{-2} [29]; Zhang et al. synthesized NiFe LDH hollow microspheres with small onset overpotential of 239 mV at a current density of 10 mA cm^{-2} and a low overpotential of 316 mV at a current density of 10 mA cm^{-2} [30]. Besides, we also use the Tafel slope to evaluate the OER performance by Tafel equation:$\eta=a+blog(j)$, where η (V) is the potential, b is the Tafel slope (mV dec^{-1})and j (mA cm^{-2}) is the current density. The results demonstrate that the Tafel slope of porous nickle-iron alloy fim is as low as 98 mV dec^{-1}, which is smaller compared with that of stainless steel mesh (152 mV dec^{-1}), suggesting nickle-iron alloy fim possess relatively excellent OER performance.

As displayed in Figure 3b, the electrochemical impedance spectroscopy (EIS) tests of nicke-iron alloy film and stainless steel mesh are investigated to further examine the sluggish charge transfer of as-prepared samples and illustrate the OER performances. It can be observed from the Nyquist plots that the solution transfer resistance (R_s) of two samples was nearly 2.2Ω. Besides, the charge transfer resistance (R_{ct}) of nicke-iron alloy film and stainless steel mesh is as low as 2.65Ω and 4.93Ω, respectively, suggesting that the nicke-iron alloy film possesses lower R_{ct} and easy sluggish charge transfer. The low R_{ct} can provide a faster OER kinetics and significantly improve the OER properties, such as lower overpotential and excellent stability. To our known, low R_{ct} can be attributed to combining electroactive material with the conductive substratre and abundant active sites which create charge transport pathways and improve electron transport [31-33].

5 Conclusions

In summary, we mention an one step electrodeposition method to prepare porous nicke-iron alloy film supported on stainless steel mesh freestanding electrode as oxygen evolution reaction catalyst. We concluded that the one step electrodeposition method has advantages for oxygen evolution reaction as follows: (1) abundant active sites and large specific surface area; (2) relatively excellent crystallinity and improved cycling stability.Nicke-iron alloy film shows a low overpotential 270 mV at a current density of 10 mA cm^{-2} and excellent electrical conductivity. We studied the OER properties of porous nickle-iron alloy films. In our paper, the nanosheets like structures provide highly exposed electrochemical active sites and large specific surface area which boost mass transport and facilitate oxygen overflow. The low cost and high catalytic activity of nicke-iron alloy film freestanding electrode provide a new strategy to fabricate alloy film for OER.

References

1. M. Dresselhaus, I. Thomas, Nature, 414, 332 (2001)
2. Y. Zheng, Y. Jiao, Y. Zhu, L.H. Li, Y. Han, Y. Chen, A. Du, M. Jaroniec, S. Qiao, Nat. Commun. 5, 3783 (2014)
3. X. Wang, W. Li, D. Xiong, D.Y. Petrovykh, L. Liu, Adv. Funct. Mater. 26, 4067 (2016)
4. Q. Lu, Y. Yu, Q. Ma, B. Chen, H. Zhang, Adv. Mater. 28, 1917 (2016)
5. F. Wang, P. He, Y. Li, T.A. Shifa, Y. Deng, K. Liu, Q, Wang, F. Wang, Y. Wen, Z, Wang, X. Zhan, L. Sun, J. He, Adv. Funct. Mater. 1602699 (2017)
6. Q. Lu, Y. Yu, Q. Ma, B. Chen, H. Zhang, Adv. Mater. 28, 1917 (2016)
7. R. Cao, W. Z. Lai, P. W. Du, Energy Environ. Sci. 5, 8134 (2012)
8. L. Han, S. Dong, E. Wang, Adv. Mater. 28, 9266 (2016)
9. H. Osgooda, S.V. Devaguptapua, H. Xub, J. Choc, G. Wu, Nano Today 11, 601 (2016)
10. E. Nurlaela, T. Shinagawa, M. Qureshi, D.S. Dhawale, K. Takanabe, ACS Catal. 6, 1713 (2016)
11. Z. Chen, J. Zhao, S. Yan, Y. Yuan, S. Liu, Mater. Lett. 157, 201 (2015)
12. X. Jia, Y. Zhao, G. Chen, L. Shang, R. Shi, X. Kang, G.I.N. Waterhouse, L. Wu, C. Tung, T. Zhang, Adv. Energy Mater. 6, 150258 (2016)
13. X. Xu, F. Song, X. Hu, Nat. Commun. 7, 12324 (2016)
14. S. Chen, J. Duan, M. Jaroniec, S. Qiao, Angew. Chem., Int. Ed. 52, 1356 (2013)
15. Y. Feng, H. Zhang, L. Fang, Y. Mu, Y. Wang, ACS Catal. 6, 4477 (2016)
16. C. Tang , H. Wang , H. Wang , Q. Zhang , G. Tian , J. Nie, F. Wei, Adv. Mater. 27, 4516 (2015)
17. C. Andronescua, S. Barwea, E. Ventosaa, J. Masaa, E. Vasiled, B.Konkenaa, S. Möllera, W. Schuhmann, Angew. Chem. Int. Ed. 56, 11258 (2017)
18. M Zhou, Q. Weng, X. Zhang, X. Wang, Y. Xue, X. Zeng, Y. Bando , D. Golberg, J. Mater. Chem. A 5, 4335 (2017)
19. X. Zhang, H. Xu, X. Li, Y. Li, T. Yang, Y. Liang, ACS Catal. 6, 580 (2016)
20. Z. Lu, W. Xu, W. Zhu, Q. Yang, X. Lei, J. Liu, Y. Li, S. Xiao, X. Duan, Chem. Sci. 50, 6479 (2014)
21. Y. Feng, H. Zhang, Y. Zhang, X. Li, Y. Wang, ACS Appl. Mater. Inter. 7, 9203 (2015)
22. J. Qi, W. Zhang, R. Xiang, K. Liu, H. Wang, M. Chen, Y. Han, R. Cao, Adv. Sci. 2, 199 (2015)
23. M. Gong, H. Dai, Nano Research 8, 23 (2015)
24. G. Wang, D. Zheng, D. Liu, J. Harris, J. Si, T. Ding, D. Qu, Electrochim. Acta 247, 722 (2017)
25. G. Liu, X. Gao, K. Wang, D. He, Jinping Li, Nano Research 10, 2096 (2017)
26. M. Yao, N. Wang, W. Hu, J. Electroanal. Chem. 782, 133 (2016)
27. C.C.L. McCrory, S. Jung, I.M. Ferrer, S.M. Chatman, J.C. Peter, T.F. Jaramillo, J. Am. Chem. Soc. 137, 4347 (2015)
28. P. He, X. Yu, X. Lou, Angew. Chem. Int. Ed. 129, 3955 (2017)

29. G. Liu, K. Wang, X. Gao, D. He, J. Li, Electrochim. Acta 211, 871 (2016)
30. C. Zhang, M. Shao, L. Zhou, Z. Li, K. Xiao, M. We, ACS Appl. Mater. Inter. 8, 33697 (2016)
31. M. Yao, N. Wang, W. Hu, J. Mater. Sci-Mater. El. 28, 11119 (2017)
32. M. Balogun, W. Qiu, H. Yang, W. Fan, Y. Huang, P. Fang, G. Li, H. Ji, Y. Tong, Energy Environ. Sci. 9, 3411 (2016)
33. M. Gong, Y. Li, H. Wang, Y. Liang, J.Z. Wu, J. Zhou, J.Wang, T. Regier, F. Wei, H. Dai, J. Am. Chem. Soc. 135, 8452 (2013)